2nd IFAC Workshop on Automatic Control in Offshore Oil and Gas Production,
May 27-29, 2015, Florianópolis, Brazil

Cost-Effective ERT Technique for Oil-in-Water Measurement for Offshore Hydrocyclone Installations

Petar Durdevic * **Leif Hansen** * **Christian Mai** *
Simon Pedersen * **Zhenyu Yang** *

* *Institute of Energy Technology, Aalborg University, Esbjerg Campus, Niels Bohrs Vej 8, 6700 Esbjerg, Denmark, e-mail: pdl@et.aau.dk, +45 31 75 13 20*

Abstract: The goal of this paper is to introduce and design a cost-effective Oil-in-Water (OiW) measuring instrument, which will be investigated for its value in increasing the efficiency of a deoiling hydrocyclone. The technique investigated is based on Electrical Resistivity Tomography (ERT), which basic principle is to measure the resistivity of substances from multiple electrodes and from these measurements create a 2-D image of the oil and gas component in the water. This technique requires the measured components to have different electrical resistances, such as seawater which has a lower electrical resistance than hydrocarbon oil and gas. This work involves construction of a pilot plant, for testing the feasibility of ERT for OiW measurements, and further exploring if this measured signal can be applied as a reliable feedback signal in optimization of the hydrocyclone's efficiency. Different algorithms for creating 2-D images and the feasibility of estimating OiW concentrations are studied and evaluated. From both steady state and continuous laminate flow perspectives, with respect to the objective which is to use this measurement for feedback control purposes.

Keywords: Electrical Resistivity Tomography, Water Treatment, Process Control, Oil in Water, Offshore.

NOMENCLATURE

Symbol	Description	Unit
Q_o	Hydrocyclone overflow flow	m^3/h
Q_i	Hydrocyclone inlet flow	m^3/h
P_i	Hydrocyclone inlet pressure	kPa
P_o	Hydrocyclone overflow pressure	kPa
P_u	Hydrocyclone underflow pressure	kPa
C_u	Concentration of oil in the underflow	mg/L
C_i	Concentration of oil in the inlet	mg/L
ϵ	Hydrocyclone efficiency	%
$i_{\alpha\beta}$	Measured current	A
$v_{\alpha\beta}$	Measured voltage drop	V
$G_{\alpha\beta}$	Measured line conductance	S
$g_{\alpha\beta}$	Line conductance pr distance	$S \cdot m$
v^{β}_{high}	Passive electrode high side voltage	V
v^{β}_{low}	Passive electrode low side voltage	V
v^{α}_{high}	Active electrode high side voltage	V
v^{α}_{low}	Active electrode low side voltage	V
r_m	Measurement resistance value	Ω
f_{frame}	2-D Frame rate of measurement	Hz
f_s	Sampling rate	Hz
n_c	Channel count	$-$
$a_{\alpha\beta}$	Coefficient of electrode-electrode line	$-$
$b_{\alpha\beta}$	Coefficient of electrode-electrode line	$-$
$c_{\alpha\beta}$	Coefficient of electrode-electrode line	$-$
$l_{\alpha\beta}$	Distance between electrodes	m
α, β	Active and passive probe designation	$-$
$\mathbf{S}$	Set of all measurements	$-$
$w_{\alpha\beta}$	Measurement weight	$-$
$\mathbf{x}$	Point in 2-D plane cross-section of pipe	m
x_1	First coordinate of electrode-electrode line	m
x_2	Second coordinate of electrode-electrode line	m
d_{min}	Minimum distance electrode-electrode line	m

⋆ Supported by the Danish National Advanced Technology Foundation through PDPWAC Project (J.nr. 95-2012-3).

1. INTRODUCTION

Hydrocyclones are commonly used to separate oil from water downstream the three phase separator in the upstream offshore oil & gas production, this means that the oil concentration which they have to handle is low as some separation has already taken place in the three phase separator. During normal North Sea operation the oil concentration exiting the three phase separator is below 5000 parts per million (PPM) or 0.5%, see Kharoua et al. (2010), while the oil concentration in a normally operating hydrocyclone's water outlet, should be around 50 PPM to 20 PPM. The goal of using hydrocyclones for produced water treatment in offshore oil & gas industry is to keep the concentration of hydrocarbon content (mainly oil part) in the treated water below 30 PPM as this is the current North Sea regulation (Miljoestyrelsen (2010)). A typical hydrocyclone consists of a cylindrical chamber to which a tangential inlet inputs a mixture of oil and water. Due to the curvature of the cylindrical shape, this fluid mixture will start to flow in a rotating path. The centrifugal forces then act on the fluid, and consequently the fluid with the higher density is pushed furthest out to the cylinder wall. The cylindrical part is connected to a long conical pipe, where at the end the water exits, this is called the *underflow* (Wolbert et al. (1995)). The conical part presses some of the lighter fluids upwards to the opposite end of

the cylindrical chamber, where a pipe of a small diameter is used to let out the oil, and this is called the *overflow* (Wolbert et al. (1995)).A schematic illustration of a typical hydrocyclone is shown in figure 1, where the paths of oil (red) and water (blue) are depicted respectively. During

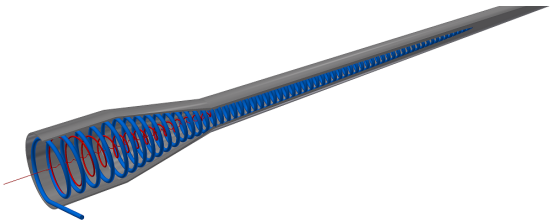

Fig. 1. A cut-trough image of the hydrocyclone, showing the hypothetical water (blue) and oil (red) paths.

normal offshore operation, the pressures at the inlet and the two outlets are measured and used to calculate the pressure drops over the inlet and the two outlets, these two pressure drops are then employed to calculate a so-called Pressure Drop Ratio (PDR) as described by equation 1, which is used to control the hydrocyclone. The PDR is correlated to the flow split Q_o/Q_i, which is the volumetric flow rate of the overflow over the volumetric flow-rate of the inflow (Husveg et al. (2007)).

$$PDR = \frac{(P_i - P_o)}{(P_i - P_u)} \tag{1}$$

It has been discovered by Husveg et al. (2007) that the flow split and the PDR can be related through a linear approximation. By adjusting the PDR and thus the flow split the controller will allow a certain amount of oil to pass through the overflow and thus ensure an efficient operation of the hydrocyclone. The PDR is linearly approximated to be proportional to the flow split, and the flow split can be further related to the efficiency which is illustrated in figure 2 (Husveg et al. (2007)). The hydrocyclone efficiency is usually defined as a percentage of the concentration of oil in the underflow C_u over the concentration of oil in the inlet C_i, resulting in the following equation $\epsilon = 1 - C_u/C_i$, see Young and Wakley (1994). This type of PDR-

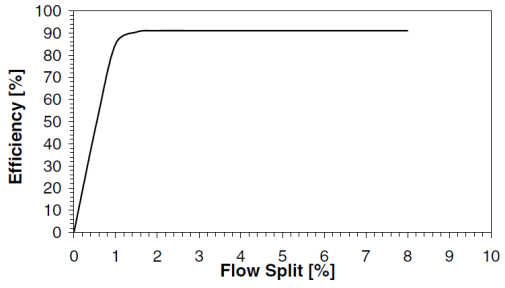

Fig. 2. Hydrocyclone efficiency related to the flow split, the result is based on an empirical analysis of a typical offshore liner (Husveg et al. (2007)).

based feedback control loop, which is the most commonly used in the offshore E&P, does not measure the OiW concentration and thus has no direct control regarding the quality of the treated water exiting the hydrocyclone. The development of the PDR control is thus done based on plenty empirical knowledge of the system, and the reference value given to the closed-loop system varies for different systems and is typicality kept at around 2-3 (Husveg et al. (2007)). One of the effective techniques commonly applied for measuring multiphase flow in the offshore industry is to separate different phases and then measure each phase individually using different single phase flow measurement (Ismail et al. (2005)), (Thorn et al. (1999)). However this kind of approach is not a directly applicable solution for feedback control of hydrocyclones, with respect to the fact that different measurements could variate and lead to some unpredictable time-delay, i.e. from the time the mixture enters the separation process until it is separated and measured. This type of measurement is more sensibly used, for example, for logic-level supervisory control or offshore evaluation. This work aims at using Electrical Resistivity Tomography (ERT) for measuring the OiW concentration at the hydrocyclone's inlet and outlets. Compared to other relevant techniques, such as γ-ray tomography, the proposed ERT technique has no use of radiation, as well as to its non-invasive and structurally robust and cost effective characteristics. Other alternative solutions could be, such as the Advanced Sensors $EX-100$ (Advanced Sensors (2014)), which uses Laser Induced UV Fluorescence to measure the amount of hydrocarbons in water. This instrument can measure in various ranges, from $0-10$ PPB, to 20.000 PPM, which can be extremely sensitive and precise. With regard to real-time purpose this instrument can have a sampling-rate of $1sec$, which could be applicable for feedback control purpose. However this type of sensoring instrument can be very expensive in a range of 30,000-40,000 USD. From our experience this equipment is difficult to calibrate in ranges of around $5-50$ PPM, mainly due to the coalescence of oil in water. Normally the test samples need to be thoroughly mixed beforehand. Other available commercial instruments, like the Agar Corporation MPFM 50 Multiphase flow meter which could be found at Agar Corporation (2014), and the Jorin VIPA which could be found at Jorin (2014). Nevertheless, all of these mentioned products are quite expensive. Thereby instead of concentrating on the usage of these sophisticated and expensive equipments, we chose to concentrate on some cost-effective electric tomography for OiW measurement, for instance, the constructed tomography sensor used in this paper costs less than 20 USD. The potential economic benefits of using cost-effective ERT for OiW concentration measurement is quite obvious. In addition, by analyzing the time-dependent tomography results, dynamic changes in the flow-rate and flow-regime can also be detected, which allows for a wide range of applications, such as slug-detection, separator and pipeline monitoring (Dong et al. (2001)). The technique is also scalable for both the pipe size and number of electrodes to suit the fidelity/resolution requirements of each individual application. In general, more electrodes would give better resolution but with slightly increased cost and computation requirements.

2. TOMOGRAPHY TECHNIQUES

Tomography is a non-invasive technique for visualizing some information over a cross-sectional segment of a pipe, which could be filled with two components with different electrical characteristics. Measurements are usually taken from several points around the pipe and the test results are then used to create a image of the segment. Tomography data can be retrieved based on different measurement techniques, such as: electrical, radioactive, optical, microwave,

ultrasonic and magnetic resonance, where the last is well known from MRI scanning used for medical imaging (Ismail et al. (2005)). Our work will concentrate on electrical tomography as this could be the cheapest and most simple technique to implement, and it is also structurally robust which is the primary objective for the offshore instruments. The application of ERT on solid-liquid hydrocyclones applied in the clay industry has been reported in Williams et al. (1999). A test setup is introduced with electrodes in several segments of the hydrocyclone such that different performances at different segments inside the hydrocyclone can be possibly observed. This work discovered that it is possible to determine if an air-core is formed inside the hydrocyclone as well as which type of underflow discharge is occurring. However the approaches and methods proposed in Williams et al. (1999) cannot be directly applied for de-oiling/liquid-liquid hydrocyclones, due to the dramatically different structural and operational characteristics of liquid-liquid hydrocyclones from solid-liquid hydrocyclones. For instance, within one of actual cases we experienced, the offshore liners often receive the flow from the separator with a maximal amount of 5% which is equal to 0.5 % mass fraction of oil in water (Kharoua et al. (2010)), while according to Williams et al. (1999), their clay hydrocyclone units receive up to 15 % mass fraction of solids. Also the pilot plant in Williams et al. (1999) involves installation of electrodes on the hydrocyclone wall. In the offshore industry this is not possible, with respect to the very high safety specifications in the constructions of equipment. We will therefore concentrate on installing the electrodes upstream the inlet and downstream the underflow of the hydrocyclone. Dong et al. (2003) investigated ERT for measuring two phase flow in pipes in terms of water and air, their results showed the potential capability of ERT instrument of measuring different types of flow regimes. They successfully distinguished between Bubble, Slug, Multi-Bubble and Annular flow. Two and three dimensional images were successfully constructed in a real-time manner. We believe that once techniques can be successfully used for gas with water, they can also be potentially used for oil with water with respect to the fact that both air and oil have very low conductivities. Hydrocarbon oil has a conductivity less than $10pS/m$ (Michael Lindner (2014)) and a gas mixture such as air has a conductivity as low as $2.95fS/m$ with high aerosol concentration (Pawar et al. (2009)). These two conductivities both have much lower values than water does, for instance the water with a salinity of $20g/kg$ and $20°C$ has a conductivity of $2.901S/m$ according to NPL (2014). Therefore these techniques could be extrapolated and used to examine OiW concentrations in evaluating deoiling system's performance. Ismail et al. (2005) pointed out some potential drawback of using electric tomography methods, i.e. their inability to send electrons in direct paths, which is different from γ-ray where the rays can be sent in a direct path from the source. Thereby using ERT, there is some risk that the electrical current from one electrode to the other through the medium may travel around obstacles of high resistivity, by following the path of least resistance. Apart from the direct path which the γ-ray tomography can handle, γ-ray tomography is also able to make fast measurements, Thorn et al. (1999) mentioned that their system developed at the University of Bergen can handle several hundred frames per second if a sufficient computing power is available. Johansen et al. (1996) mentioned the safety issue of using γ-ray tomography, though with their setup the radiation is less than $0.1\mu Svh^{-1}$ at 1 meters distance, with is far below the recommended maximum dose of $7.5\mu Svh^{-1}$. To achieve this low radiation, the setup described in Johansen et al. (1996) requires carefully construction using thick steel plates to shield the radiation. Although the γ-ray method has some advantages over the electric tomography, as shown in figure 3, it won't be the main focus in this work, mainly due to the complexity of design and the high price of it.

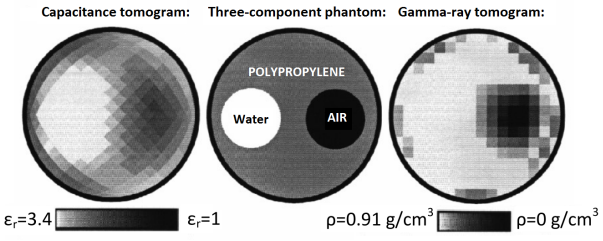

Fig. 3. Compassion between ECT and γ-ray tomography, the test benchmark is illustrated as the middle image. The γ-ray tomography can be improved to show the water phase (Johansen et al. (1996)).

3. TEST SETUP

The ERT method is, from the manufacturing perspective, cheap and easy to construct, however it requires direct electrical connection to the pipe contents thereby this method requires the use of somewhat specific materials. The resolution of the method depends on the permissible number of electrodes. The test setup is constructed to enable the liquid to be stationary and to be flowing subject to a pumping system. This setup consists of several parts: the ERT pipe which is constructed out of polymethyl methacrylate (PMMA, acrylic glass) with a nominal diameter of $50mm$ and $30cm$ length; a centrifugal pump; connecting pipes with an inner diameter of $12mm$ and a buffer tank. A schematic diagram of the test setup is illustrated in figure 4. Water and oil can be added to the system by filling up the buffer tank. The electrodes have been placed

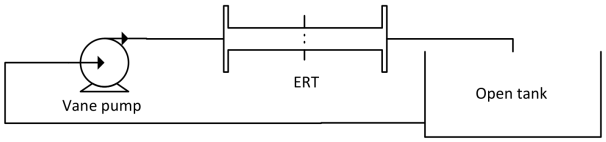

Fig. 4. Diagram of the test system, containing a controllable pump, and the ERT unit which is connected to a I/O card. (National instruments PCI-6229)

around the pipe in 360 degrees to cover the entire circle. 12 electrodes are placed 30° apart, as illustrated in figure 5. The electrodes are threaded stainless steel rods of equal length, which can be adjusted by screwing and whereto the measurement connections are made using cable clamps. Further mounting improvement could be achieved by using machined non-reactive metal electrodes (for example platinum, titanium or "Hastelloy", depending on the process conditions), similar to the design and materials used in magnetic flow meters, see Emerson (2014). Each electrode is connected to a digital voltage source through a precision

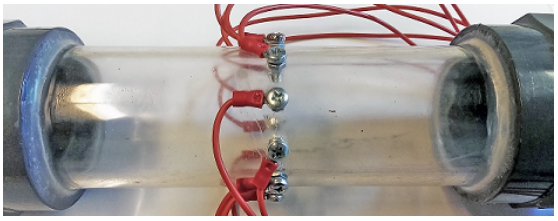

Fig. 5. Illustration of the ERT sensor configuration

±1% measurement resistor, where each end of the resistor is connected to an ADC channel on the NI PCI-6229 data acquisition card, as illustrated in figure 6. Conductance

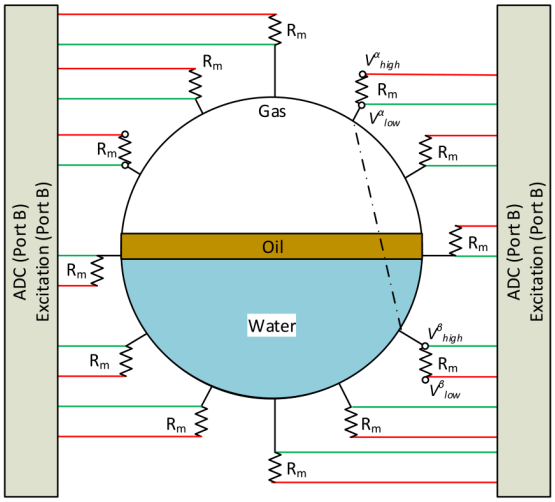

Fig. 6. Probe layout and electrical connection with measurement resistors for ERT setup. Red wires represent excitation/measurement connections and green wires represent passive measurement connections

measurement is performed by exciting one electrode at 5 volts while all the other electrodes are set to 0 volts, then measuring the voltage on all channels including the excitation channel. The conductance for one electrode pair, $G_{\alpha\beta}$, can then be calculated as in equations 2 to 4. α represents the active electrode while β represents the passive electrode, such that v^{α}_{high} and v^{α}_{low} is the high add low voltages respectably for the measurement resistor at the active electrode, and v^{β}_{high} and v^{β}_{low} is for the measurement resistor at the passive electrode, see figure 6.
Similarly $i_{\alpha\beta}$ is the current through the passive electrode β wile α is the active electrode, and $v_{\alpha\beta}$ is the voltage drop from α to β.

$$i_{\alpha\beta} = \frac{v^{\beta}_{high} - v^{\beta}_{low}}{R_m} \tag{2}$$

$$v_{\alpha\beta} = v^{\alpha}_{low} - v^{\beta}_{high} \tag{3}$$

$$G_{\alpha\beta} = \frac{i_{\alpha\beta}}{v_{\alpha\beta}} \tag{4}$$

After one measurement frame is completed, the same procedure will be repeated for all other electrodes. By the end $12 \cdot 11 = 132$ (channel) samples are collected. These measurements can be performed at a maximal sampling rate of $f_s = 1000[Hz]$, which is subdivided over the channel count $n_c = 16$ (due to coding specifics, 4 extra channels are scanned but not connected to electrodes), so that each full measurement cycle (frame) can be performed at a rate as: $f_{frame} = \frac{f_s}{n_c} = 62.5[Hz]$. This sampling rate can be increased by using equipment with a faster analog converter, if this is required by the application.

4. TOMOGRAM GENERATION ALGORITHMS

In the following, two algorithms, which are based on a 2-D plane representing the cross-section of the pipe in which all the electrodes are situated, are considered. The origin corresponds to the center of the pipe, the x_1-axis represents the width of the pipe, the x_2-axis represents the height of the pipe. The radius of the pipe is normalized to 1. The position of each electrode is represented by a point in this plane. For each pair of the active and the passive electrode (α, β), a standard line equation in the form of equation 5 is defined for the line trough these points.

$$a_{\alpha\beta}\, x_1 + b_{\alpha\beta}\, x_2 + c_{\alpha\beta} = 0 \tag{5}$$

Each of the measured conductances is multiplied with the distance between the electrodes, $l_{\alpha\beta}$, in order to get a conductance per normalized length unit (radius), $g_{\alpha\beta}$.

$$g_{\alpha\beta} = G_{\alpha\beta}\, l_{\alpha\beta} \tag{6}$$

For each point in the plane, $\mathbf{x}$, an interpolated conductance per length unit, $g(\mathbf{x})$, is calculated as a weighted average of $g_{\alpha\beta}$, which is inspired by Shepard's method, see Shepard (1968).

$$g(\mathbf{x}) = \begin{cases} \dfrac{\sum\limits_{(\alpha,\beta)\in\mathbf{S}} w_{\alpha\beta}(\mathbf{x}) g_{\alpha\beta}}{\sum\limits_{(\alpha,\beta)\in\mathbf{S}} w_{\alpha\beta}(\mathbf{x})} \end{cases} \tag{7}$$

$$\mathbf{S} = \{(\alpha,\beta) | \beta \neq \alpha\} \tag{8}$$

In this $\mathbf{S}$ is the set of all measurements represented by its pair of electrodes, and the weight, $w_{\alpha\beta}(\mathbf{x})$ is defined as:

$$w_{\alpha\beta}(\mathbf{x}) = \frac{1}{D_i\,(\mathbf{x}, \alpha, \beta)^u} \tag{9}$$

Where the constant u controls how much the influence of each measurement decreases with distance. According to Shepard (1968) $u = 2$ is suggested, while Łukaszyk (2004) noted that $u > 2$ usually is assumed and $u > 1$ is needed for a smooth interpolation function. $D_i(\mathbf{x}, \alpha, \beta)$ is one of two different distance quantities denoted either $D_{dis}(\mathbf{x}, \alpha, \beta)$ or $D_{\mathbf{L}uk}(\mathbf{x}, \alpha, \beta)$, these quantities are what makes the two algorithms different in our concern. Both quantities are related to the minimum distance, $d(\mathbf{x}, \alpha, \beta)$, from a point, $\mathbf{x}$ to the line defined for a pair of electrodes (α, β) (see figure 7):

$$d(\mathbf{x}, \alpha, \beta) = \frac{|a_{\alpha\beta}\, x_1 + b_{\alpha\beta}\, x_2 + c_{\alpha\beta}|}{\sqrt{a^2_{\alpha\beta} + b^2_{\alpha\beta}}} \tag{10}$$

$D_{dis}(\mathbf{x}, \alpha, \beta)$ is the maximum between $d(\mathbf{x}, \alpha, \beta)$ and a

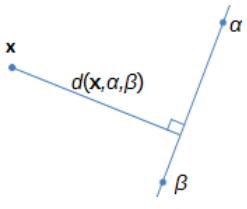

Fig. 7. Relation between $\mathbf{x}$, α, β and $d(\mathbf{x}, \alpha, \beta)$

lower bound for the distance d_{min}, which is used in order not to over emphasize the value of a single $g_{\alpha,\beta}$ for points on the line defined for the corresponding pair of electrodes (α, β):

$$D_{dis}(\mathbf{x}, \alpha, \beta) = \max\left(d(\mathbf{x}, \alpha, \beta), d_{min}\right) \tag{11}$$

The algorithm that applies this quantity is noted as: Minimum distance algorithm in this paper. $D_{\text{Łuk}}(\mathbf{x}, \alpha, \beta)$ is an adaptation of Łukaszyk-Karmowski probability metric for a distance between two random vectors according to Łukaszyk (2004). A new set of axes is defied with the projection of $\mathbf{x}$ on the line for $g_{\alpha\beta}$ as origin, the y_1-axis is on the line and has positive direction from α to β, the y_2-axis is particular on the y_1-axis and has positive direction from the line to $\mathbf{x}$. The point $\mathbf{x}$ is described by Dirac delta distributions, i.e. an exact value:

$$f_{\mathbf{x},1}(y_1) = \delta(y_1) \tag{12}$$

$$f_{\mathbf{x},2}(y_2) = \delta(y_2 - d(\mathbf{x}, \alpha, \beta)) \tag{13}$$

While the line is described by an uniform distribution on the line and a Dirac delta distribution particular on it:

$$f_{l,1}(y_1) = \begin{cases} \frac{1}{z_\alpha + z_\beta} y_1 & \text{if} - z_\alpha \leq y_1 \leq z_\beta \\ 0 & \text{otherwise} \end{cases} \tag{14}$$

$$f_{l,2}(y_2) = \delta(y_2) \tag{15}$$

Where z_α and z_β are the distance from the point's projection on the line to the active and passive electrode respectively. The definition of $D_{\text{Łuk}}(\mathbf{x}, \alpha, \beta)$ in equation 16 is valid for independent marginal distributions.

$$D_{\text{Łuk}}(\mathbf{x}, \alpha, \beta) \equiv \left(\sum_{i=1}^{2} \left(\int_{-\infty}^{\infty} \int_{-\infty}^{\infty} f_{\mathbf{x},i}(y_a) f_{l,i}(y_b) \, \mathrm{d}y_a \mathrm{d}y_b \right)^p \right)^{\frac{1}{p}} \tag{16}$$

Where p defines which p-norm is used to get the norm of the vector, as this vector represents a physical distance the 2-norm is most commonly used, resulting in equation 17.

$$D_{\text{Łuk}}(\mathbf{x}, \alpha, \beta) = \left(\left(\frac{z_\alpha^2 + z_\beta^2}{2 \cdot (z_\alpha + z_\beta)} \right)^p + d(\mathbf{x}, \alpha, \beta)^p \right)^{\frac{1}{p}} \tag{17}$$

The algorithm that applies this quantity is noted as: Łukaszyk-Karmowski algorithm in this paper.

5. TEST PROCEDURE AND CALIBRATION

Two test scenarios are considered: (i) static testing, where the ERT-pipe is filled with liquid consisting of a predetermined water & oil contents with a mixture ratio of 15/85%, which we name as low water case, and 85/15% which we name as high water case. The static tests are used as the baseline for exploring the capabilities of the setup; (ii) dynamic flowing test, where the pipe is subjected to a liquid flow, in order to investigate the dynamic performance of the measurement solution. Ideally an oil & water mixture would have been used, however due to limitations in the pumping system the dynamic flow rate test contains water and a small gas phase (air) within this early investigation phase, where the air is existing solely due to turbulence in the pipes; no dedicated gas flow was added to this test. In order to calibrate the electrode connections, the pipe is filled with water, and the electrodes are manually adjusted by screwing until the measured conductivity per length in all paths are the same.

6. TEST RESULTS AND DISCUSSION

The obtained results for stationary low water levels are illustrated in figures 8 and 9, and the high water level results are illustrated in figures 10 and 11. By comparing both concerned algorithms, it is evident that the Łukaszyk-Karmowski algorithm can lead to more smooth results (in the terms of the gradient), whereas in the minimum distance approach, the results are affected by the electrode positions, as compared from figures 8a and 9a. However the smoothing of the Łukaszyk-Karmowski algorithm results in a transient between conductive and non-conductive material having a lesser gradient than in the minimum distance cases, as illustrated from the comparison of figures 8b and 9b. This increases the difficulty of determining the phase separation from the 2-D results if a gradient based approach is utilized. Another option is to estimate the water fraction using a simple threshold on the conductance values over the set of points χ, as shown in equation 18.

$$w_{water} = \frac{\sum_{\mathbf{x} \in \chi} (g(\mathbf{x}) > g_{thres})}{n_x} \tag{18}$$

Where the threshold g_{thres} is selected from the largest transition of the minimum distance algorithm in the low water case, where the transition is easily determined. In these experiments the threshold becomes $1.236 * 10^{-}5$. Applying the equation to the results yields the water fractions listed in table 1. It is observed that the tests

Experiment	Low water	High water
Minimum distance	8.5 %	87.6 %
Łukaszyk-Karmowski	12.1 %	87.7 %

Table 1.

with high concentration of water have worse results than the tests with a high concentration of oil/gas, here referring to figures 8a, 8b, 9a, 9b, 10a, 10b, 11a and 11b. We observed that the conductivity transition (high-low), which is illustrated the following 1-D figures 8b, 9b, 10b and 11b, is occurring more prominently for the low water concentration tests than the high water concentration tests. To illustrate this refer to the gradient of the slope in figures 8b and 9b, where the slope has a high gradient and where it is lower in figure 11b, which represents the high water concentration calculated using the minimum distance algorithm. It has a similar gradient as figures 8b and 9b, although the oil water transition is more curved when observing the 2-D figure 10a. A possible reason for this behavior is that only a small amount of oil/gas around the electrodes results in almost 0 conductivity measurement, thus the oil/gas is more likely to effect a high water concentration than the opposite. This effect is worsened with a lower amount of electrodes, as this leaves relatively big gaps between electrodes and thus the transition where oil occurs on the electrodes will be larger, and the results will have a less precise illustration of the phases during high water phase concentrations. For the test with mixed gas/water flow, illustrated in figure 12 and 13 the individual gas bubbles cannot be distinguished from the liquid due to the low resolution using either method, which is critical if the gas bubble sizes are to be directly determined, however the overall content of the pipe is well represented as being mostly conductive material. The mean conductance, which is calculated and presented in figures 8a, 8b, 9a, 9b, 10a, 10b, 11a, 11b, 12 and 13, can be used for determination of the pipe contents. However this is heavily effected by several factors, including salinity and oil composition, therefore some form of calibration or secondary measurement will be needed to allow this value to be used for control and monitoring purposes. An investigation of the mean conductance of the low water level in figure 8a ($0.35348 \cdot 10^{-5}$), the mean conductance

of the high water level in figure 10a ($2.1784 \cdot 10^{-5}$) and the mean conductance of the running water and gas mixture from figure 12 ($2.3279 \cdot 10^{-5}$) indicate that there is a logical relation between the mean conductance and the amount of water in the pipe. This means that it is indeed feasible to use this technique for measuring the concentration of water/oil or water/gas in the pipes.

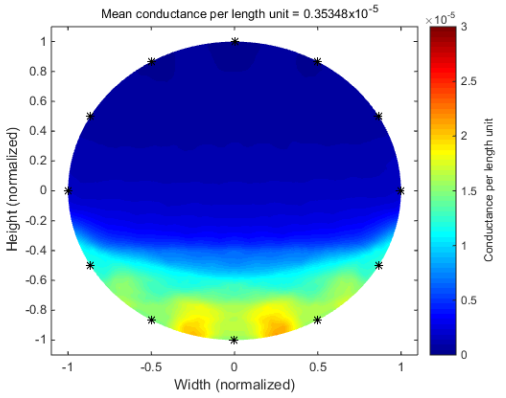

(a) Minimum distance algorithm, 2D

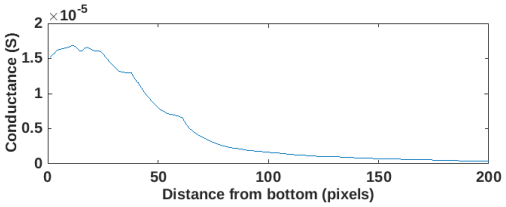

(b) Minimum distance algorithm, average levels

Fig. 8. Low water level using minimum distance algorithm

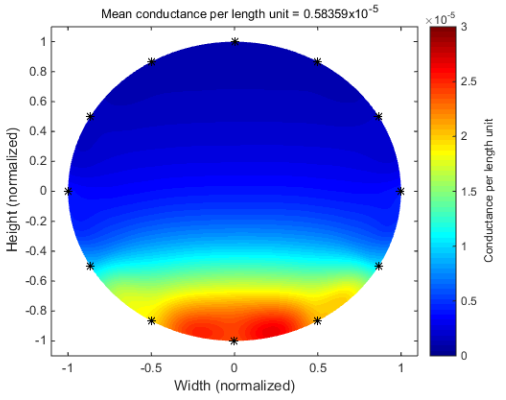

(a) Łukaszyk-Karmowski algorithm, 2D

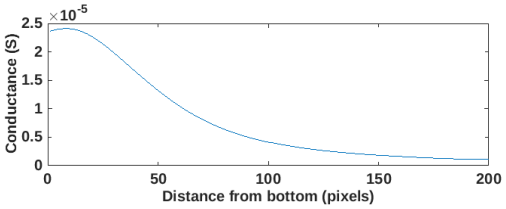

(b) Łukaszyk-Karmowski algorithm, average over width

Fig. 9. Low water level using Łukaszyk-Karmowski algorithm

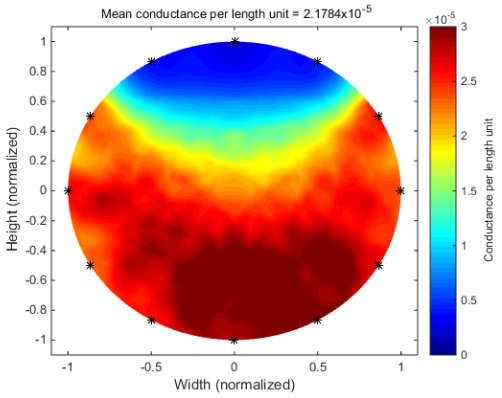

(a) Minimum distance algorithm, 2D plot

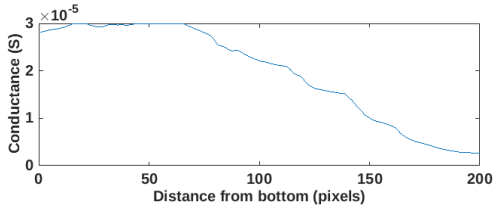

(b) Minimum distance algorithm, average levels

Fig. 10. High water level using minimum distance algorithm

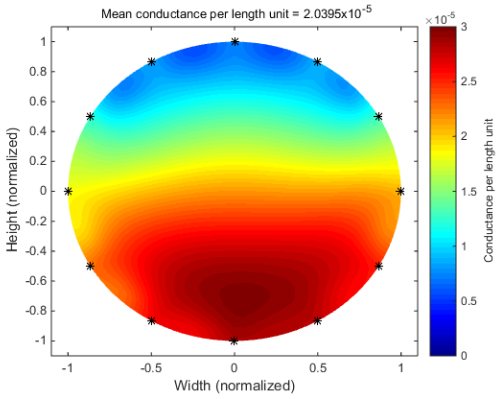

(a) Łukaszyk-Karmowski algorithm, 2D

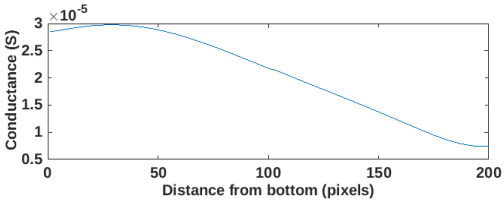

(b) Łukaszyk-Karmowski algorithm, average levels

Fig. 11. High water level using Łukaszyk-Karmowski algorithm

7. CONCLUSION

In this preliminary study, a cost-effective and non-invasive method based on ERT technique for OiW measuring and analysis has been investigated. The ultimate objective of this undergoing investigation aims for a potential cost-effective real-time measurement technique for OiW concentration at the hydrocyclones inlet and underflow. To test the feasibility of the proposed method and approach,

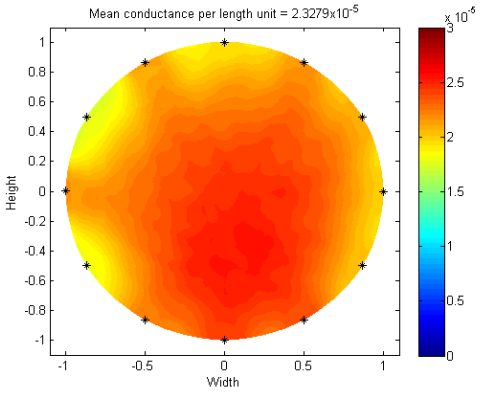

Fig. 12. Running water and gas mixture using minimum distance algorithm, 2-D

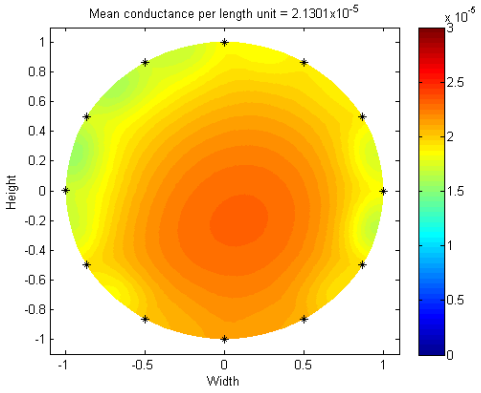

Fig. 13. Running water and gas mixture using Łukaszyk-Karmowski algorithm, 2-D

a pilot plant consisting of a 50mm pipe with attached electrodes and a pumping circulatory system, is constructed. The oil and water interface in the pipe for static cases can be clearly observed in the generated 2-D tomograms. For dynamic flow measurements, where the medium was water with a small amount of non-purposed gas mixture, the overall content of the pipe can still be determined. Trough analysis of the average conductivity in the mixture, we are able to detect a link between OiW concentration and the average of measured conductivities.

Future work will involve testing of the concentration of oil/gas in water of known concentrations to investigate if concentrations can be registered precisely, thus simplifying the use of 2-D imaging for feedback control. Another extend of our work will be to increase the amount of electrodes to allow for higher resolution and thus investigate if this will enable us to visualize small particles in 2-D images. Also electric capacitive tomography (ECT) will be investigated, to compare the merits of this technology with ERT.

ACKNOWLEDGEMENTS

The authors would like to thank the support from the Danish National Advanced Technology Foundation. Our thanks also goes to colleagues J.P. Stigkjær, A. Aillos, K. G. Nielsen, M. Haubjerg and P. Molinari from Maersk Oil A/S, colleagues P. Sørensen, A. Andreasen, B. Løhndorf, S. A. Meybodi and J. M. Holm from Ramboll Oil & Gas A/S, and H. Enevoldsen from AAU, for many valuable discussions and technical support.

REFERENCES

Advanced Sensors (2014). Advanced Sensors - Oil in Water Analyzers. URL `http://www.advancedsensors.co.uk/`.

Agar Corporation (2014). Agar Corporation - MPFM 50. URL `http://www.agarcorp.com/Animation/MPFM/50/MPFM50.html`.

Dong, F., Jiang, Z., Qiao, X., and Xu, L. (2003). Application of electrical resistance tomography to two-phase pipe flow parameters measurement. *Flow Measurement and Instrumentation*, 14(4-5), 183–192.

Dong, F., Liu, X., Deng, X., Xu, L., and Xu, L.a. (2001). Identification of two-phase flow regimes in horizontal, inclined and vertical pipes. *Measurement Science and Technology*, 12(8), 1069–1075.

Emerson (2014). Magnetic flowmeter material selection guide. URL `http://www2.emersonprocess.com/siteadmincenter/PM%20Rosemount%20Documents/00816-0100-3033.pdf`.

Husveg, T., Rambeau, O., Drengstig, T., and Bilstad, T. (2007). Performance of a deoiling hydrocyclone during variable flow rates. *Minerals Engineering*, 20(4), 368–379.

Ismail, I., Gamio, J., Bukhari, S., and Yang, W. (2005). Tomography for multi-phase flow measurement in the oil industry. *Flow Measurement and Instrumentation*, 16(2-3), 145–155.

Johansen, G., Frøystein, T., Hjertaker, B.T., and Olsen, O. (1996). A dual sensor flow imaging tomographic system. *Measurement Science and Technology*, 7(3), 297–307.

Jorin (2014). Jorin - Vipa product range. URL `http://www.jorin.co.uk/products/`.

Kharoua, N., Khezzar, L., and Nemouchi, Z. (2010). Hydrocyclones for De-oiling Applications—A Review. *Petroleum Science and Technology*, 28(7), 738–755.

Michael Lindner (2014). Oil condition monitoring using electrical conductivity, oelcheck gmbh. URL `http://www.machinerylubrication.com/Read/29407/oil-condition-monitoring`.

Miljoestyrelsen (2010). Status for den danske offshorehandlingsplan til udgangen af 2009. *Miljoestyrelsen*.

NPL (2014). Physical properties of sea water. URL `http://www.kayelaby.npl.co.uk/general_physics/2_7/2_7_9.html`.

Pawar, S., Murugavel, P., and Lal, D. (2009). Effect of relative humidity and sea level pressure on electrical conductivity of air over indian ocean. *Journal of Geophysical Research: Atmospheres (1984–2012)*, 114(D2).

Shepard, D. (1968). A two-dimensional interpolation function for irregularly-spaced data. In *Proceedings of the 1968 23rd ACM National Conference*, ACM '68, 517–524. ACM, New York, NY, USA.

Thorn, R., Johansen, G., and Hammer, E. (1999). Three-Phase Flow Measurement in the Offshore Oil Industry: Is There a Place for Process Tomography? *Industrial Process Tomography*, 228–235.

Łukaszyk, S. (2004). A new concept of probability metric and its applications in approximation of scattered data sets. *Computational Mechanics*, 33(4), 299–304.

Williams, R.A., Jia, X., West, R.M., Wang, M., Cullivan, J., Bond, J., Faulks, I., Dyakowski, T., Wang, S., Climpson, N., Kostuch, J., and Payton, D. (1999). Industrial monitoring of hydrocyclone operation using electrical resistance tomography. *Minerals Engineering*, 12(10), 1245–1252.

Wolbert, D., Ma, B.F., Aurelle, Y., and Seureau, J. (1995). Efficiency estimation of liquid-liquid Hydrocyclones using trajectory analysis. *AIChE Journal*, 41(6), 1395–1402.

Young, G. and Wakley, W. (1994). Oil-water separation using hydrocyclones: An experimental search for optimum dimensions. *Journal of Petroleum Science and Engineering*, 11(93), 37–50.